# Modelling 2D complex anomalies by seismic tomography (detection and delineation of anomalies with sharp boundaries)

E. Cardarelli

(Received: March 13, 2007; accepted: September 13, 2007)

***ABSTRACT*** In seismic tomography an important task is to delineate the shape and geometry of anomalies with sharp boundaries. This is especially true when building structures are investigated. In this paper properties and characteristics of some seismic inversion algorithms to individuate the best one for solving such a problem are analyzed. At first, some considerations about the inversion theory are discussed, then the inversion programs used are described in detail and two new algorithms are implemented. For a better understanding of the problem, a synthetic example is carried out. Finally, a seismic tomography survey is performed to asses the thickness of a brick wall that forms the sides of a flowerpot. The inversion of the collected data set of both the synthetic model and the field survey are performed by all the algorithms considering straight ray path approximation, and results are discussed and compared. The use of a variable damping factor seems to be a good method to determine anomalies for reducing ghosts and artefacts. The new algorithms permit us to insert a starting model and the use of inequality constraint in such a way that the results better approximate a realistic model. In the field survey a comparison with ray tracing is made.

## 1. Foreword

In the field of applied geophysics, tomographic techniques are not only a valid tool for determining properties on sites of large engineering plants, but are an important aid in the evaluation of the state of conservation of ancient monuments, especially thanks to their own high resolution characteristic (Cardarelli, 2002; Cardarelli *et al*., 2002). In particular electrical tomography is generally used to individuate boundary anomalies characterised by a high resistivity contrast with respect the surrounding material; on the other hand seismic tomography is useful to determine elastic parameters of building structures and evaluate their degree of decay (Carrion, 1991; Olson *et al.,* 1993; Jalinoos *et al.,* 1994; Cardarelli, 1995; Cardarelli and de Nardis, 2001; Louis *et al*., 2002; Cardarelli and Cerreto, 2002). Generally, when natural soils are investigated anomalies show a gradual velocity contrast, on the contrary when building structures are studied sharp variations of velocities are generally present between targets and surrounding materials, this is because, depending on the building technique, in general, different materials are in touch with different elastic characteristics. In this frame, to delineate and evaluate the shape and geometry of the anomalies could be important to plan the restoration that follows. For this purpose, a comparison between different algorithms was performed in order to individuate the one that is more suitable to delineate shape and evaluate dimensions of anomalies; a synthetic model and a case history were considered.

 

## 2. Theory and background

It is well known that the solution of the inverse problem depends mainly on both the field data set and the geophysicist's knowledge about the investigated area, as well as some hypotheses concerning physics and geometric characteristics of the subsoil.

For this reason the solution of the inverse problem is a compromise between the numeric solution obtained by the processing of the data set and the solution that the geophysicist considers to be the most probable thanks to the knowledge of the surveyed area. For this reason, a priori information is without doubt one of the main parameters used to stabilize the system and to direct the solution towards a solution as close to the true model as possible. In this ambit, it is possible to consider both physical parameters (inequality constraints, starting model, etc.) and mathematical ones (damping factor, weight and roughness matrix, etc.). In the last twenty years, in this frame, a large number of algorithms were implemented and tested (Dines and Little, 1979; Lines and Treitel, 1984; Paige and Saunders, 1982; Van der Sluis and Van der Vorst, 1987; Pilkington and Todoeschuck, 1992; Clippard *et al*., 1995).

In this study, direct methods and iterative methods that take into account both physical and mathematical stabilizers were used.

### *2.1. Direct methods*

It is well known that the solution for an over determined system can be looked on to detect the minimum of the functional:

$$\Psi(\mathbf{c}) = \left(\mathbf{d} - \mathbf{G}\mathbf{c}\right)^T \left(\mathbf{d} - \mathbf{G}\mathbf{c}\right) \tag{1}$$

where **d** is the vector of the data set, **G** is the solution matrix, **c** the vector of unknowns and $T$ indicates the transpose.

The solution for Eq. (1) is the Gauss normal equation:

$$\mathbf{c} = \left(\mathbf{G}^{\mathbf{T}}\mathbf{G}\right)^{-1} \mathbf{G}^{\mathbf{T}}\mathbf{d} \tag{2}$$

If the damping factor and the mean slowness are added (a priori information) Eq. (2) can be written as:

$$\mathbf{c} = \left[\mathbf{G}^{\mathbf{T}}\mathbf{G} + \lambda\mathbf{I}\right]^{-1} \mathbf{G}^{T}\mathbf{d} + \left[\mathbf{G}^{\mathbf{T}}\mathbf{G} + \lambda\mathbf{I}\right]^{-1} \lambda\bar{c}, \tag{3}$$

where $\lambda$ is the damping factor, **I** the identity matrix and $\bar{c}$ the mean slowness of the investigated area.

To increase stability of the system without reducing the null space, the variable damping factor can be used (Bernabini and Cardarelli, 1997)

$$\mathbf{c}=\left[\mathbf{G}^{\mathrm{T}}\mathbf{G}+\mathbf{A}\right]^{-1}\mathbf{G}^{\mathrm{T}}\mathbf{d}+\left[\mathbf{G}^{\mathrm{T}}\mathbf{G}+\mathbf{A}\right]^{-1}\mathbf{A}\bar{c}, \tag{4}$$

where $\mathbf{\Lambda}$ is the diagonal matrix of damping factors, other parameters have the same meaning as in Eq. (3).

In the case where some elements of the investigated area are known it is possible to add to the functional a vector of slowness that we consider to be the more probable

$$\mathbf{c}=\left[\mathbf{G}^{\mathrm{T}}\mathbf{G}+\mathbf{A}\right]^{-1}\mathbf{G}^{\mathrm{T}}\mathbf{d}+\left[\mathbf{G}^{\mathrm{T}}\mathbf{G}+\mathbf{A}\right]^{-1}\mathbf{A}\mathbf{C}^{*}, \tag{5}$$

where **C*** is the diagonal matrix of the slowness, other parameters have the same meaning as in Eq. (3).

Eqs. (3), (4) and (5) were used to investigate the one that is able to delineate a better shape and geometry of seismic anomalies, the algorithms are respectively named TOMO1, TOMO2, and TOMO3.

### *2.2. Iterative methods*

It is possible to demonstrate that images with sharp boundaries can be recovered by regularized inversion algorithms based on a new family of stabilizing function. Particularly minimum support (MS) and minimum gradient support (MGS). These new stabilizers select inverse models within the class of models with minimum volume of domain with anomalous parameter distribution (MS stabilizer) or with the minimum volume of area where the gradient of the model parameter is non-zero (MGS stabilizer). These classes of models describe compact objects (minimum support) or objects with sharp boundaries (minimum gradient support) that are a typical target in geophysical archaeological exploration ( Zhdanov and Tolstaya, 2004; Zhdanov *et al*., 2005).

To verify this sentence, an implementation of the minimum support inversion was performed (Last and Kubik, 1983).

Minimum support stabilizer, is proportional to the area of the non-zero values of the difference between the current model $m$ and an appropriate a priori, model $m_{apr}$

$$S_{MS}(m)=\int_{v}\frac{(m-m_{apr})^2}{(m-m_{apr})^2+e^2}dv \qquad e^2<<(m-\boldsymbol{m}_{apr})^2, \tag{6}$$

where $e$ is the focusing parameter and $V$ some volume in the Earth (Zhdanov and Tolstaya, 2004). In numerical form Eq. (6) is

$$s_{MS}(m)=\left(m-m_{apr}\right)^{T}\left[\left(\hat{m}-\hat{m}_{apr}\right)^2+e^2\hat{I}\right]^{-1}\left(m-m_{apr}\right) \tag{6a}$$

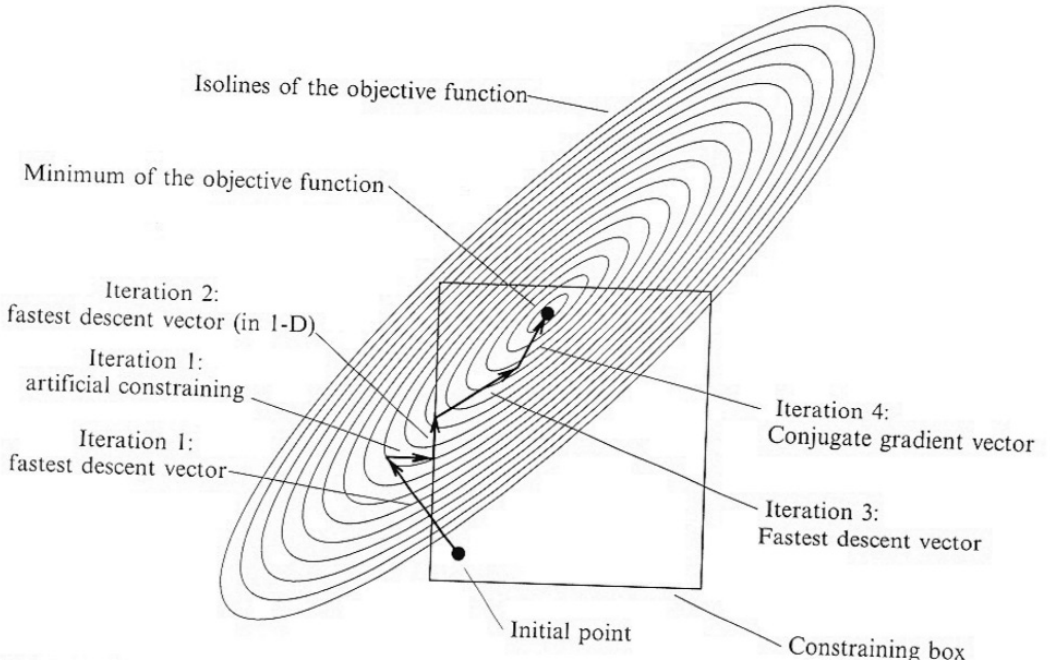


Fig.1 - Constrained minimization of a quadratic objective function [after Ditmar, (2002)].

where $\hat{m}$ and $\hat{m}_{apr_r}$ are $N_m$ x $N_m$ diagonal matrices of inverse model parameters

$$\hat{m} = \text{diag}\,(m_1, m_2, \ldots m_{Nm}) \qquad \hat{m}_{apr_r} = \text{diag}\,(m_{1apr}, m_{2apr}, \ldots m_{Nmapr})$$

Finally, the last algorithm that was studied and implemented is based on the structural inversion (SI) idea (Ditmar, 2002), in this case the model is represented by a rectangular grid. The simplest way to develop a gridded model with sharp features is to constrain the solution such that the value in each cell must lie within a certain interval (Barbosa *et al.,* 1999). The idea of Ditmar (2002) is based on the hypothesis that the slownesses are known and the unknowns are the parameters that describe the function of the shape of the anomaly. In this case, the question was inverted assuming that the shape and dimensions of the anomalies are known and the slowness are unknowns. The proposed algorithm proceeds as the conventional conjugate-gradient method with certain components of the solution vector being frozen; the components get frozen or unfrozen during the inversion.

This process is performed in three steps, as illustrated with a simple 2D example [Fig.1, after Ditmar (2002)]. At each iteration the solution ($m_{original}$) must fit the constraints, i.e. lie within the constraining box. If some components of the solution vector are beyond predetermined limits at a certain moment, these components are subject at first step to artificial constraining, i.e. are updated in compliance with the formula

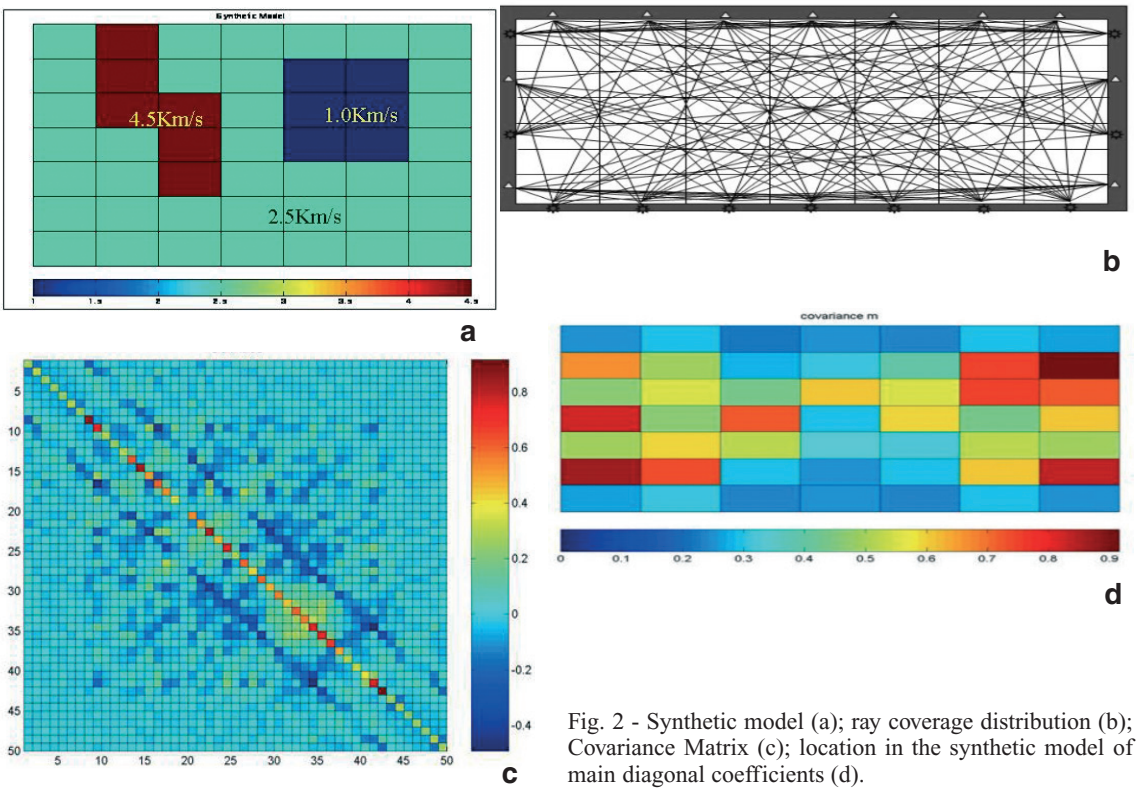


Fig. 2 - Synthetic model (a); ray coverage distribution (b); Covariance Matrix (c); location in the synthetic model of main diagonal coefficients (d).

$$m_{constrained} = \begin{cases} m_{\min} & if \quad m_{original} < m_{\min} \\ m_{original} & if \; m_{\min} \le m_{original} \le m_{\max} \\ m_{\max} & if \quad m_{original} > m_{\max} \end{cases}. \tag{7}$$

In Fig. 1, constraining along the horizontal direction takes place after the first iteration.

The second step consists of analysing these components. A component, directed outwards from the constraining interval, will push, at the next iteration, the corresponding component of the solution out of the constraining interval, again. To prevent this, these components are switched off.

The third step has the job of switching-on the component. For example, the horizontal direct component in Fig. 1 is switched on after the second iteration.

## 3. Synthetic example

To determine the algorithm that provides best results in the case of sharp boundary anomalies a synthetic model was created. Travel times were calculated considering a ray's straight path approximation. In the model, two anomalies respectively of 1.0 km/s and 4.5 km/s are surrounded

from material characterized from mean velocity of 2.5 km/s (Fig. 2a).

Shots and geophones are uniformly arranged around the structures (11 geophones and 11 shots), a total of 121 travel times were considered (Fig. 2b). A random type noise (non-organized), was added to the theoretical travel times (no Gaussian data). This addition represents the recurrence of casual noise that experimental reading might contain (box error of 10%).

The following was used

$$T' = T + (rnd - 0.5) \times T \times K, \tag{8}$$

where $T'$ is the value of the travel time with added noise, $T$ is the value of synthetic travel times, *rnd* is a random function that generates a casual number from 0 to 1 of equal probability (box car distribution), $K$ varies the percentage of synthetic travel times. The area is divided into 49 cells (Fig. 2a).

For a better understanding of the system, the well-known covariance matrix (CM) with damping factor $\lambda$=0.1 is calculated (Fig. 2c)

$$CM = \left(G^T G\right)^{-1} \tag{9}$$

where **G** is the solution matrix of the system and $T$ indicates the transposition. In the hypothesis of uncorrelated data for this matrix, the analysis of its main diagonal provides the degree of error amplification that occurs in the inversion, and by analysing the elements off the main diagonal, correlation degree between each cell with respect to all the others is given (Menke, 1989).

With dumping CM is (Aki and Lee, 1976) :

$$\mathbf{CM} = \left(\mathbf{G^T G} + \lambda \mathbf{I}\right)^{-1} \mathbf{G^T G} \left(\mathbf{G^T G} + \lambda \mathbf{I}\right)^{-1} = \left(\mathbf{G^T G} + \lambda \mathbf{I}\right)^{-1} \mathbf{R}^T, \tag{9a}$$

where **R** is Data Resolution Matrix defined as:

$$\mathbf{R} = \left(\mathbf{G^T G} + \lambda \mathbf{I}\right)^{-1} \mathbf{G^T G}. \tag{9b}$$

In Fig. 2d, the values of the main diagonal of the CM are located in the area to individuate the ill conditioned cells.

### *3.1. Data processing and results*

The data set was inverted by using the algorithms described in the previous paragraph. In Table 1, the parameters used for each program are reported.

In Fig. 3a, the field velocity obtained with TOMO1 is shown, in this case a constant damping factor ($\lambda$=0.1) and mean velocity equal to 2.5 km/s were considered as a priori information as

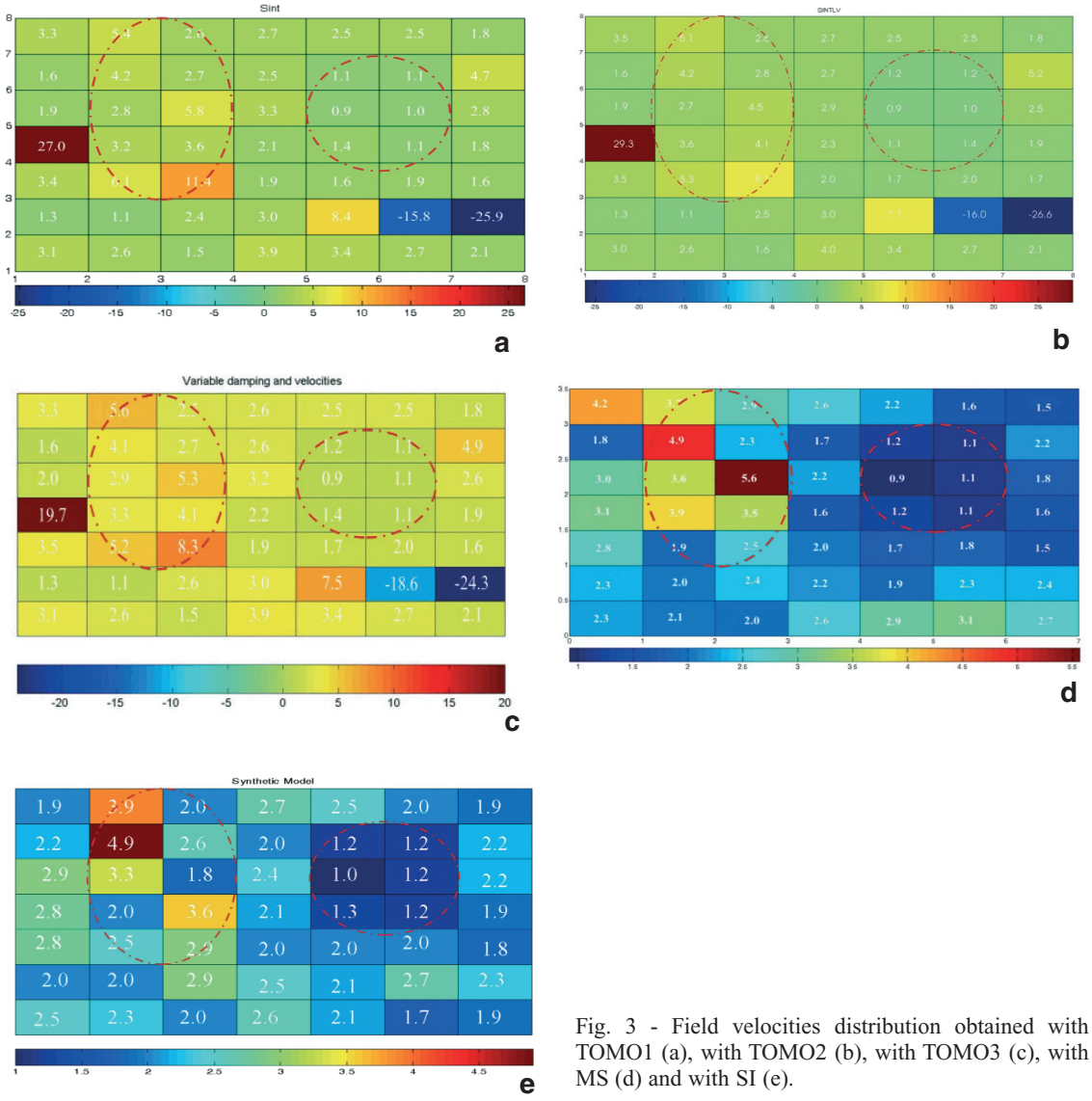


Fig. 3 - Field velocities distribution obtained with TOMO1 (a), with TOMO2 (b), with TOMO3 (c), with MS (d) and with SI (e).

well as to stabilize the system, both anomalous areas are detected (bounded zones with ellipse curves) even if the low velocity values are better identified, ghosts are present in the area where a covariance matrix detected ill-conditioned cells. The choice of the best damping factor was determined by the L curve method (Bernabini and Cardarelli, 1997). In Fig. 3b, the distribution of velocities obtained by TOMO2 are shown. The inversion was performed considering variable damping factors ($\lambda_1$=0.1, $\lambda_2$=0.01, $\lambda_3$=0.3) respectively, for the background velocity, the low velocity anomaly and the high velocity anomaly when a constant mean velocity was considered as a priori information ($V_1$=2.5 km/s). Also, in this case, the choice of the best damping factor was determined by the L curve method. Ghosts are present in the same zones, both low velocity zones are better identified as being higher with respect to TOMO1. Fig. 3c shows the results of

Table 1 - Parameters used for algorithms TOMO1, TOMO2, TOMO3, MS and SI in the synthetic model. $\lambda_1$, $\lambda_2$, $\lambda_3$, damping factors, $V_1$, $V_2$, $V_3$, mean velocities used in the inversions.

| Algorithm | $\lambda_1$ damping | $\lambda_2$ damping | $\lambda_3$ damping | $V_1$ km/s | $V_2$ km/s | $V_3$ km/s | Costraints$_1$ | Costraints$_2$ | Costraints$_3$ | e focusing parameter |
|---|---|---|---|---|---|---|---|---|---|---|
| Tomo 1 | 0.1 | - | - | 2.50 | - | - | - | - | - | - |
| Tomo 2 | 0.1 | 0.01 | 0.3 | 2.50 | - | - | - | - | - | - |
| Tomo 3 | 0.1 | 0.01 | 0.3 | 2.50 | 1.5 | 5.0 | - | - | - | - |
| MS | 0.1 | - | - | 2.47 | - | - | - | - | - | 0.003 |
| S I | - | - | - | 2.00 | - | - | 1.8<m<5 | 0.8<m<1.2 | 1.5<m<3.0 | |

TOMO3. In this case the inversion was performed considering both variable damping factors ($\lambda_1$=0.1, $\lambda_2$=0.01, $\lambda_3$=0.3) and variable velocities ($V_1$=2.5 km/s, $V_2$=1.5 km/s, $V_3$=5 km/s). The values of ghosts are made smaller but the anomalous zones are not well identified. In Fig. 3d, the results of MS are shown; the inversion process was carried out using a damping factor $\lambda$=0.1 focusing parameter $e$=0.003 and a starting homogeneous model $V$=2.47 km/s, in this case, the ghosts are reduced and the anomalous zones are well detected. Finally, in Fig. 3e the field velocity performed with SI is displayed; the inversion was performed starting with a homogeneous model $V$=2.0 km/s and using different inequality constraints for each area where the velocities are different; a 1.5<$V$<3.0 km/s interval for the surrounding area, 1.8<$V$<5 km/s for the high velocity anomaly and 0.8<$V$<1.2 km/s for the low-velocity anomaly. In this case, the artefacts vanish and both anomalous zones are quite well detected. This emphasizes the fact that the error distribution, in this case, is not Gaussian while the least squares methods give optimal results only when data noises follow a Gaussian distribution. The practice of geophysical inversion shows, that least squares solutions are very sensitive for sparsely distributed large errors (outliers) in the data set and the estimated model parameters may even be completely unphysical. (Dobroka *et al*., 2007). This is the reason why, in some pixel, no realistic solution is present in the algorithms when any constraints are used, furthermore these ghosts are mainly located where CM identified ill conditioned cells.

This is to underline that the model that is close to the realistic model obtained with the SI algorithm does not show the lower root mean square $\sigma$:

$$\sigma = \sqrt{\frac{1}{M}\sum_{j=1}^{M}(t_f^j - t_c^j)^2}$$

where $M$ is the number of the data, $t_f$ is the data field and $t_c$ is the calculated one.

The lower value is the one obtained with TOMO1 $\sigma$=0.1 whilst $\sigma$=0.19 with MS algorithm and with SI $\sigma$=0.29.

Such values demonstrate that in these cases the minimum is flat and results depend on the starting model and physical and mathematical stabilizers.

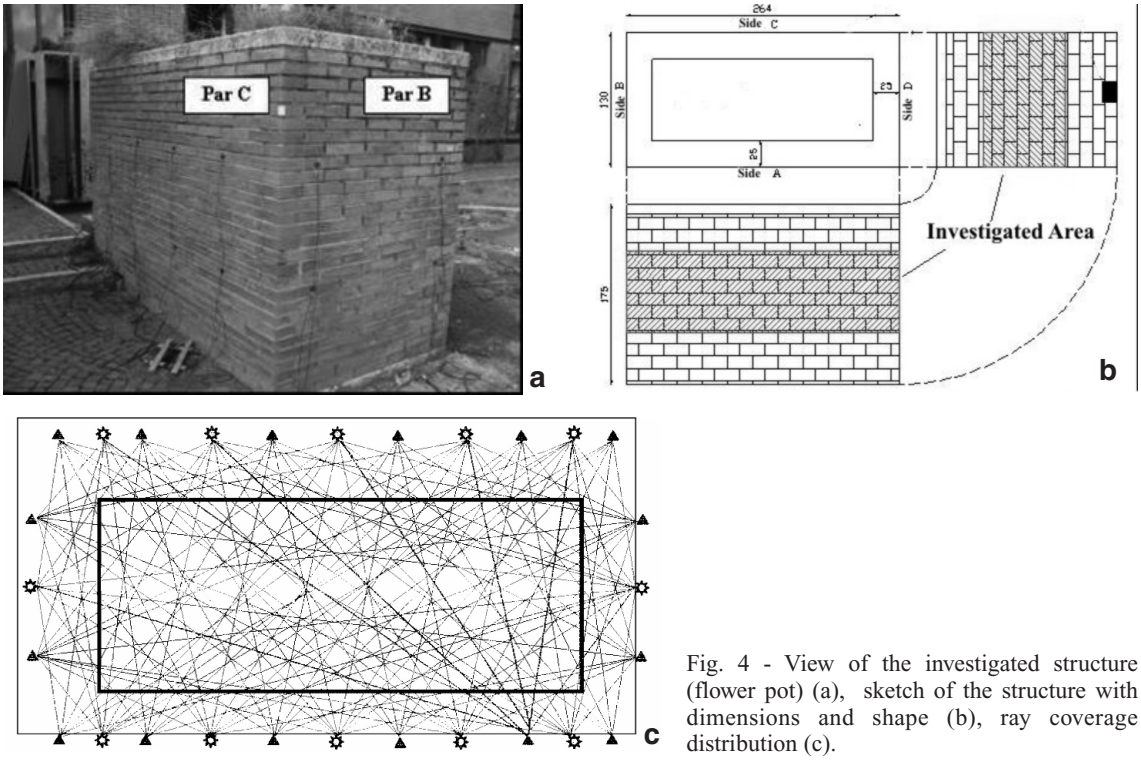


Fig. 4 - View of the investigated structure (flower pot) (a), sketch of the structure with dimensions and shape (b), ray coverage distribution (c).

In Table 1, the parameters used during the inversion process for each program, are summarized.

## 4. Test site

To thoroughly analyze this problem a survey aiming at determining the thickness of a brick wall that forms the sides of a flowerpot was performed. In Fig. 4a, a picture of the investigated object is shown with the dimensions of the map of Fig. 4b. The flower pot is filled with ground, the expected velocity of the bricks is approximately 2.0-2.5 km/s and the velocity of the ground about 1.0 km/s. Seismic tomography was carried by using sixteen 4 kHz cut-off frequency piezoelectric accelerometers and 12 shots located around the pot, the collected data set was formed by 176 travel times (Fig. 4c), the area was divided into 32 cells. In Fig. 5, an example of picking of a seismogram is shown.

### *4.1. Data processing and results*

Different algorithms were compared also for a field survey, TOMO1 was excluded because no reliable results in the synthetic example were given back; tomographies are shown in Fig.6. In Table 2, the parameters used during the inversion process for each program are summarized.

In Fig. 6a, the field velocities obtained from TOMO2 are shown, in this case some ghosts exist. The inner low-velocity zone is quite well identified even if some cells on the top side, where

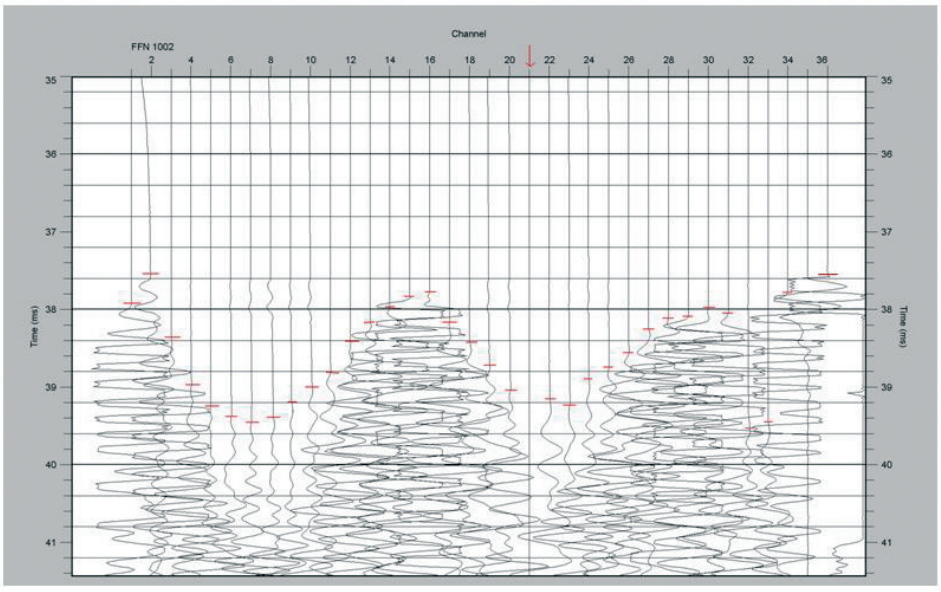


Fig. 5 - Example of seismogram recorded in the survey of a flower pot. The picking is manually executed.

bricks are present, show lower velocity values. Fig. 6b shows the results of TOMO3, in this case the number of artefacts are reduced even if higher values are displayed, a similar trend to the previous tomography is obtained.

In Fig. 6c, the field velocity obtained with MS is shown; in this case, ghosts are made to disappear and the inner zone is quite well solved even if some cells on the left of the figure present higher velocity values (1.9 km/s) and the brick wall shows lower values (1.1 km/s) on the top.

Finally, in Fig. 6d, results of SI are shown, in this case, is evident that the result is greatly improved, in fact, the ghosts have disappeared and the velocities are quite congruent with the studied material. To compare results obtained with a straight ray-path approximation, ray tracing was performed using Linear Travel Time Interpolation (LTI ) by Asakawa and Kawanaka (1993),

Table 2 - List of the used parameters for algorithms TOMO2, TOMO3, MS and SI at the test site. $\lambda_1$, $\lambda_2$, damping factors, $V_1$, $V_2$, mean velocities used in the inversion.

| Algorithm | $\lambda_1$ damping | $\lambda_2$ damping | $V_1$ km/s | $V_2$ km/s | Costraints$_1$ | Costraints$_2$ | e focusing parameter |
|---|---|---|---|---|---|---|---|
| Tomo 2 | 0.1 | 0.3 | 1.60 | - | - | - | - |
| Tomo 3 | 0.1 | 0.3 | 2.50 | 1.0 | - | - | - |
| MS | 0.1 | - | 1.64 | - | - | - | 0.003 |
| S I | - | - | 2.00 | 1.0 | 1.5<m<2.5 | 0.8<m<1.2 | |

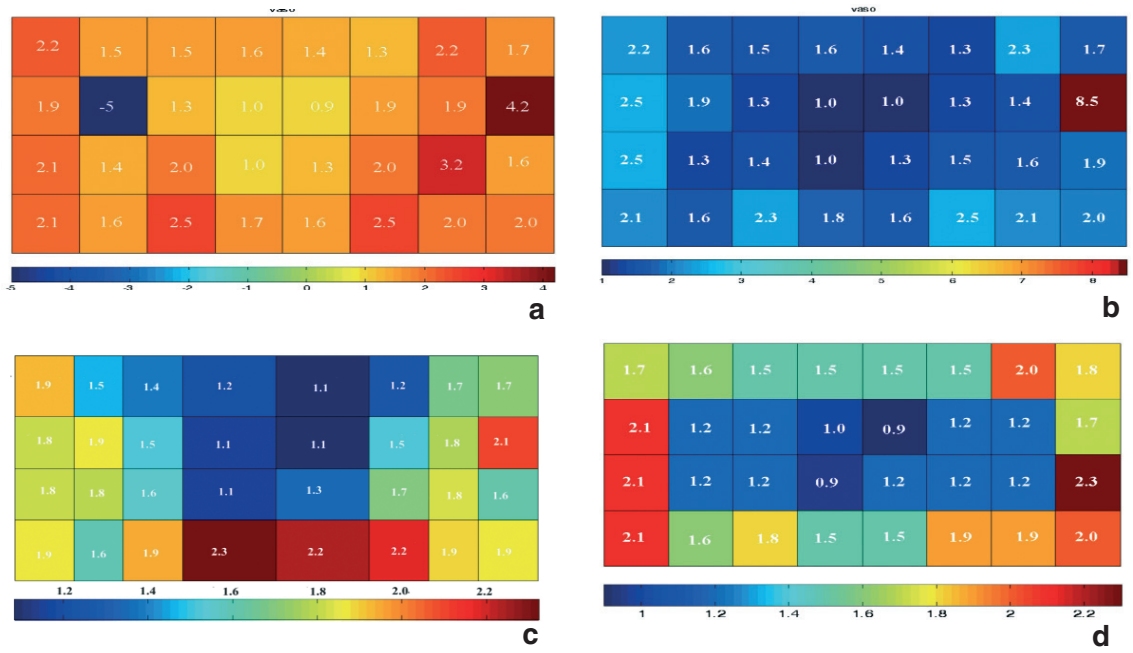


Fig. 6 - Field velocitie distribution obtained with TOMO2 (a), with TOMO3 (b), with MS (c), with SI (d).

the inversion was carried out by Biconjugate Gradient (BCG) (Press *et al*., 1992). The inversion was performed starting with a homogenous model and considering the same cell distribution as other inversions (Fig. 7). The results are in agreement with the SI algorithm confirming the inner lower velocity zone ranging in the interval between 0.9-1.2 km/s, the brick wall shows zones with lower velocities than 2.0 km/s, and the r.m.s. is lower than other algorithms used with straight rays ($\sigma$=0.19). It is to be considered that the pot is about twenty years old and some bricks show fractures and decay degrees, this fact could justify the lower velocity values detected in some

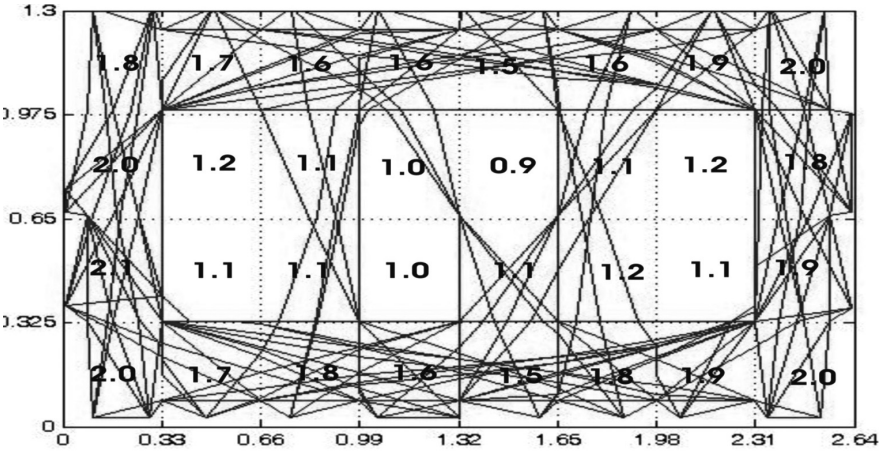


Fig. 7 - Field velocities distribution obtained with BCG and ray tracing.

places of the wall during the inversion.

It should be underlined that if a priori information of the structure is well defined and elastic characteristics are known with a good degree of reliability, the intervals of the inequality constraint parameters in the S.I. algorithm can be reduced, consequently, the range of variability of the velocities of the anomalies will be reduced.

## 5. Conclusions

To determine the dimensions and the shape of sharp boundary velocity anomalies in building structures is very important in the ambit of successive restoration plans, for this reason, to identify the algorithm that can solve this kind of problem is without doubt a useful tool.

In this frame, some conclusions can be made at the end of this study, at first, especially in the case of building structures, a deep knowledge of the studied material is a good starting point for the inversion process.

The use of variable damping factors (TOMO2) is a good method for stabilizing the system without reducing the null space such as the use of the velocity variable matrix (TOMO3).

A minimum support seems to be a good compromise between the quality of the results and time consuming processing. The algorithm is very easy to use and the inversion process is fast.

Structural inversion by using inequality constraints allows us to reach a better quality of results with respect the other algorithms, it is true especially if we have a posteriori information obtained from other inversion processes. For this reason, the use of different algorithms with different characteristics permits us to create a procedure to obtain a more realistic model, step by step. For example, to define the interval of velocities of the anomalies with TOMO2 or TOMO3 and to delineate the shape with MS can be useful to determine inequality constraints and dimensions and the geometry of the anomalies for the SI algorithm. A ray tracing approach is without doubt more suitable and gives best results in all cases where high contrast between velocities exists. We can conclude by stating that the r.m.s. is too weak a parameter to indicate the best solution in terms of physical model.

## REFERENCES

Aki K. and Lee W.H.K.; 1976: *Determination of three-dimensional velocity anomalies under a seimic array using first P arrival times from local earthquakes, I, a homogeneous initial model.* Journal of Geophysical Research, **81**, 4381-4399.

Asakawa E. and Kawanaka T.; 1993: *Seismic ray tracing using linear travel time interpolation.* Geophysical Prospecting, **41,** 99-111.

Barbosa V.C.F., Silva J.B.C. and Medeiros W.E.; 1999: S*table inversion of gravity anomalies of sedimentary basins with non smooth basement relief and arbitrary density contrast variations.* Geophysics, **64**, 754-764.

Bernabini M. and Cardarelli E.; 1997: *Variable damping factor in travel time tomography* Journal of Applied Geophysics, **38**, 131-141.

Cardarelli E.; 1995: *3D tomography of some pillars of the Coliseum.* Boll. Geof. Teor. App., **37**, 257-265.

Cardarelli E. and De Nardis R.; 2001: *Seismic refraction, isotropic anisotropic seismic tomography on an ancient monument (Antonino e Faustina temple AD 141)*. Geophysical Prospecting, **49**, 228-240.

Cardarelli E.; 2002: *Geoelectric survey by ERT to investigate marble ruins at the Roman Forum, Rome Italy.* European J. Env. Eng. Geophys., **7**, 219-228.

Cardarelli E. and Cerreto A.; 2002: *Ray tracing in elliptical anisotropic media using the linear travel time interpolation (LTI) method applied to travel time seismic tomography.* Geophysical Prospecting, **50**, 55-72.

Cardarelli E., Godio A., Morelli G., Sambuelli L., Santarato G. and Socco L.V.; 2002: *Integrated geophysical surveys to investigate the Scarsella vault of St. John's Baptistery in Florence.* The Leading Edge, **21**, 467-470.

Carrion P.; 1991: *Dual tomography for imaging complex structures* Geophysics, **56**, 1395-1404.

Clippard J.D., Christensen D.H. and Rechtien R.D.; 1995: *Composite distribution inversion applied to crosshole tomography.* Geophysics, **60**, 1283-1294.

Dines K.A. and Little R.J.; 1979: *Computerized geophysical tomography.* In: Proc. IEEE 67 (7).

Ditmar P.; 2002: *Finding the shape of local heterogeneity by means of structural inversion with constraints.* Geophysical Prospecting, **50**, 209-223.

Dobroka M., Ormos T. and Gyulai A.; 2007: *On the reduction of noise-sensitivity in seismic tomography.* In: 13th European Meeting of Environmental and Engineering Geophysics, Istanbul Turkey. Extended Abstract.

Jalinoos F., Olson L.D., Aouad M.F. and Balch A.H.; 1994: *Acoustic tomography for QNDE of structural concrete.* In: Quantitative Non-destructive Evaluation (QNDE). Proceeding, 14 Iowa State University.

Last B.J.J. and Kubik K.; 1983: *Compact gravity inversion.* Geophysics, **48**, 713-721.

Lines L.R. and Treitel S.; 1984: *Tutorial - A review of least-squares inversion and its application to geophysical problems.* Geophysical Prospecting, **32**, 159-186.

Louis I.F., Karastathis C.V., Vafidis P.A.and Louis F.I.; 2002: *Resistivity Modelling and Imaging Methods for Mapping Near-Surface Features: Application to a Site Characterization at the Ancient Temple of Olympian Zeus in Athens.* Journal of the Balkan Geophysical Society, **5**, 135-144.

Menke W.; 1989: *Geophysical data analysis: discrete inverse theory.* Academic Press, New York, 289 pp.

Olson L.D., Jalinoos F., Aouad M.F. and Balch A.H.; 1993: *Acoustic tomography and reflection imaging for non-destructive evaluation of structural concrete.* NSF Phase I Final Report (Award No. 9260840), SBIR Industrial Innovation Interface Division, Washington D.C.

Paige C.C. and Saunders M.A.; 1982: LSQR: *An algorithm for sparse linear equations and sparse least squares.* In: ACM Transactions on Mathematics Software, New York U.S.A., pp. 43-71.

Pilkington M. and Todoeschuck J.P.; 1992: *Natural Smoothness constraints in cross-hole seimic tomography.* Geophysical Prospecting, **40**, 227-242.

Press H.V., Tenkolsky S.A., Vetterling W.T. and Flannery B.P.; 1992: *Numerical recipes in Fortran.* Cambridge University Press, 2nd Edition, 993 pp.

Van der Sluis A. and Van der Vorst H.A.; 1987: *Numerical solutions of large sparse algeabric systems arising from tomographic problems.* In: Nolet G. (ed), Seismic Tomography, Springer, Dordrecht, pp. 49-83.

Zhdanov M. and Tolstaya E.; 2004: *Minimum support nonlinear parameterization in the solution of a 3D magnetotelluric inverse problem.* Inverse Problem, **20**, 937-952.

Zhdanov M., Vignoli G. and Ueda T.; 2005: S*harp boundary inversion in crosswell travel-time tomography.* J. of Geophysics and Engineering, **3**, 122-134.

*Corresponding author:* Ettore Cardarelli
Dip. di Idraulica, Trasporti e Strade
Università "La Sapienza"
via Eudossiana 18, 00184 Roma, Italy
phone: + 39 06 44585079; fax: + 39 06 44585080; e-mail: ettore.cardarelli@uniroma.it